Complex deformation pattern of the Pamir–Hindu Kush region inferred from multi-scale double-difference earthquake relocations

2 authors, including:

Ling Bai
Chinese Academy of Sciences
30 PUBLICATIONS **191** CITATIONS

Some of the authors of this publication are also working on these related projects:

Project   The earthquake activity and deep structure of the earth in the Himalayan-Tibetan region View project

Project   seismology View project

Focal depths and mechanisms of shallow earthquakes in the Himalayan–Tibetan region

CrossMark

Ling Bai *, Guohui Li, Nangyal G. Khan, Junmeng Zhao, Lin Ding

Key Laboratory of Continental Collision and Plateau Uplift, Institute of Tibetan Plateau Research, Chinese Academy of Sciences, Beijing 100101, China

A B S T R A C T

The complexity of the Himalayan–Tibetan lithospheric deformation is evident from widespread seismicity and diverse focal mechanism solutions. Here we investigate the focal depths and fault plane solutions of 97 moderate and shallow earthquakes in the Himalayan–Tibetan region by modeling teleseismic P-wave and its tailing surface reflections pP and sP. Earthquakes in central Tibet are restricted to the upper crust and originate dominantly by strike-slip faulting, in agreement with the low P-wave velocity layers in the lower crust and the strong S-wave attenuation zones in the uppermost mantle. In northern and southern Tibet, where the Asian and Indian plates descend beneath central Tibet, earthquakes appear to be distributed throughout the thickness of the crust and exhibit dominantly reverse faulting. We incorporate well-estimated focal depths of 127 additional earthquakes from previous studies to estimate the seismogenic thickness (*Ts*) of the study region. The resulting pattern of *Ts* is found to be rather flat for central and northeastern Tibet and highly variable along the strike of the Himalayan foreland.

© 2015 International Association for Gondwana Research. Published by Elsevier B.V. All rights reserved.

1. Introduction

The collision between the Indian and Eurasian Plates followed by the subduction and closure of the Neo-Tethys Ocean formed the Himalayas and the Tibetan plateau, the world's largest orogenic belt and highest plateau (Fig. 1). The elevation of the Tibetan plateau exceeds 5 km within an area of 2,500,000 km^2 (Amante and Eakins, 2009). Its crust is 50–80 km thick, nearly twice as much as the average Moho depth of the world (Shin et al., 2009). From north to south the Kunlun, Songpan-Ganze, Qiangtang, and Lhasa terranes exemplify the remarkable horizontal inhomogeneity of the plateau (Yin and Harrison, 2000).

The United States Geological Survey (USGS) earthquake catalog includes about 1500 shallow (H ≤ 50 km) earthquakes and 700 intermediate-depth (50 < H ≤ 300 km) earthquakes with M_W > 5.0 from the past 50 years (Fig. 2). Since 1900, 8 earthquakes of M_W ≥ 8.0 and 52 earthquakes of 7.0 ≤ M_W < 8.0 have occurred (Hatzfeld and Molnar, 2010). The whole region of the plateau accommodates shallow earthquakes, while intermediate-depth seismicity is concentrated at the Indo-Burma and Pamir-Hindu Kush subduction zones, which are located at the eastern and western Himalayan syntaxes, respectively. The diversity of focal mechanism solutions for both shallow and intermediate-depth earthquakes indicates intricacy of the current stress field beneath the Himalayan–Tibetan region.

The significant differences between earthquake catalogs illustrate that the routine measurements of earthquake source parameters are highly uncertain, especially for shallow earthquakes (Fig. 3). The catalog from China Earthquake Network Center (CENC) relies on arrival times of regional seismic network which provides a good constraint on focal depths for earthquakes within the network. However, differences in depth estimates for nearly 15% of earthquakes are larger than 20 km due to scarce station coverage and complex velocity structure in the Himalayan–Tibetan region (Fig. 3(a1)). The USGS preliminary determination of epicenters (PDE) provides earthquake catalog based on arrival times of teleseismic body waves. This catalog is as much accurate as that of CENC catalog because the combination of later phases improves the accuracy of the earthquake locations (Fig. 3(b1)). The global Centroid Moment Tensor (gCMT) locations are updated USGS PDE locations using low-pass-filtered long-period waveforms (Ekström et al., 2012) (Fig. 3(c1)). The EHB catalog provides the best depth estimates based on various teleseismic arrival times for earthquakes up to the end of 2008 (Engdahl et al., 1998). Focal depths are better constrained by modeling the broadband waveforms as the depth phases are easily distinguishable than in long-period records.

Location accuracy of focal depths directly affects our understanding about the physical mechanism of the seismicity and the deep structure of the Earth. The controversy on the lower crustal or upper mantle earthquakes beneath the Himalayan region comes from the measurement uncertainty of the earthquake location and the crustal thickness (Chen and Yang, 2004; Jackson et al., 2008). A detailed investigation of the crustal flow layer, which is distinguished from the seismogenic zone, requires accurate knowledge of the earthquake location
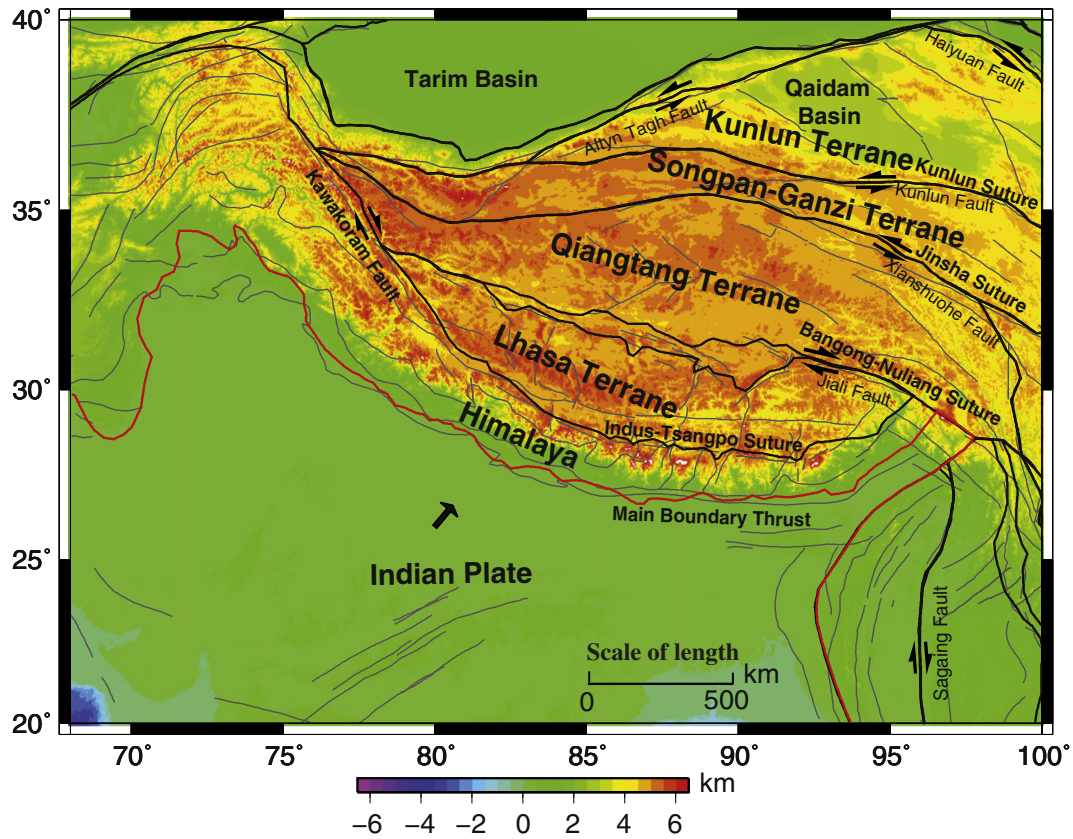

Fig. 1. Tectonic map of the Himalayan–Tibetan region. Red and black lines are plate and terrane boundaries, respectively.

(Klemperer, 2006). Similarly, understanding the structure of subducted slab requires constrains from earthquake location and focal mechanism solutions (Bai and Zhang, 2015).

In this paper, we estimate focal depths and focal mechanism solutions of 97 shallow earthquakes in the Himalayan–Tibetan region using teleseismic P-wave modeling. These 97 events account for more than 95% of moderate earthquakes (5.4 ≤ M_W < 7.0) occurred since 1990. These events occurred at different regions hence suitable for providing constrains for various tectonic implications. The manifold implications of this study would provide new constrains on the deep

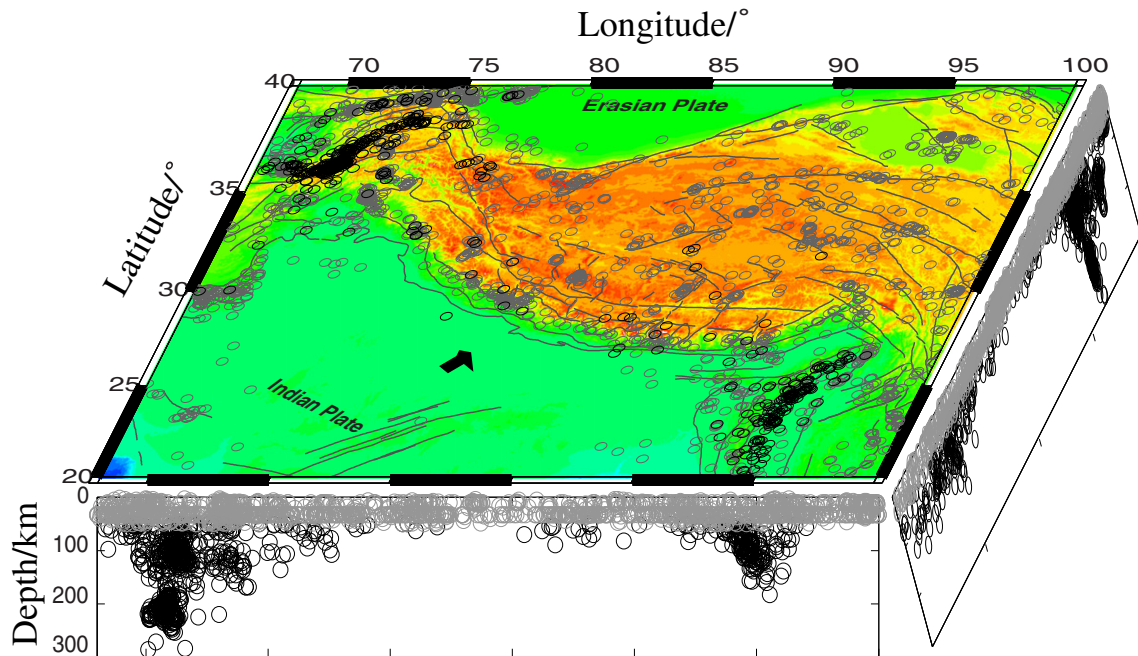
Fig. 2. Distribution of earthquakes of Mw ≥ 5.0 that occurred in the past 50 years. Gray and black circles show shallow and intermediate-depth earthquakes, respectively. The depth scales in cross-sections are twice of the actual size.
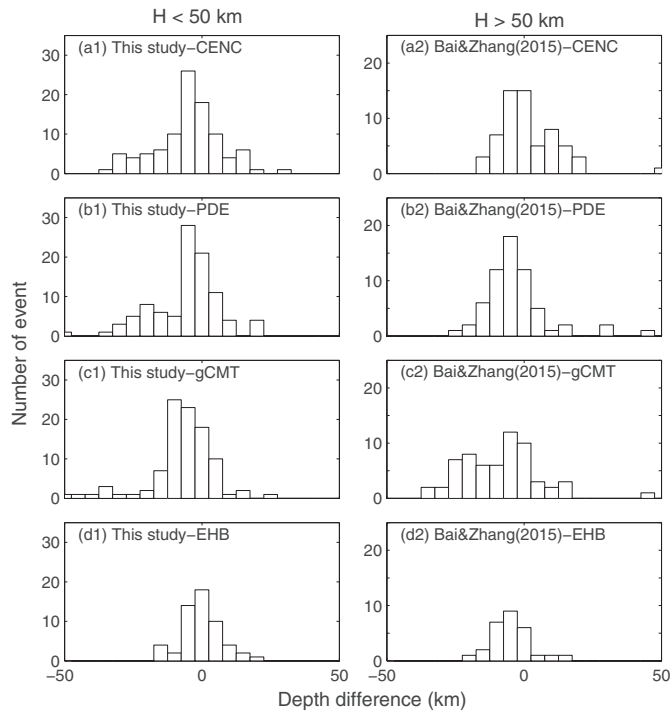
Fig. 3. Comparison of focal depths between different catalogs. (a1)–(d1) show depth differences of shallow earthquakes between those obtained in this study and those listed in CENC, USGS PDE, gCMT, and EHB catalogs. (a2)–(d2) show depth differences of intermediate-depth earthquakes between those obtained in Bai and Zhang (2015) and listed in above catalogs.

structures of the Earth beneath the Himalayan–Tibetan region in more detail.

2. Waveform data and modeling

We collected data for all earthquakes in the Himalayan–Tibetan region with waveforms available at the Incorporated Research Institutions for Seismology (IRIS) Data Management Centre. We examined vertical-component recordings from stations at epicentral distances between 30° and 90° (Fig. 4) in order to avoid interference from core phases and upper mantle triplications. We acquired the earthquakes with relatively simple source time functions but sufficiently high signal-to-noise ratios. Waveforms are band-pass-filtered from 0.03 to 1 Hz and deconvolved from the station response.

We employed teleseismic waveform inversion methods developed by Kikuchi and Kanamori (1982), which involve matching of complete P waveforms to synthetic waveforms. This procedure assumes that the source can be represented as a point (the centroid) in space and a series of overlapping triangles in time. We calculate synthetic waveforms using four-layer velocity and density model for the upper, middle, lower crust and mantle structures along with variable Moho depth of 35–80 km based on CRUST2.0 (Bassin et al., 2000), except for the structures that have been imaged in more detail through seismic experiments (Maggi et al., 2000; Mejia, 2001; Rai et al., 2006). Amplitudes are corrected for geometrical spreading using attenuation t* operator with a value of 1.0 s. As the reflection points of pP and sP phases are located on the surface of the Earth, the topography is corrected in order to obtain focal depths relative to the sea level.

Based on our experiment on the velocity structure, we found that source depth estimates are primarily controlled by the pP-P and sP-P
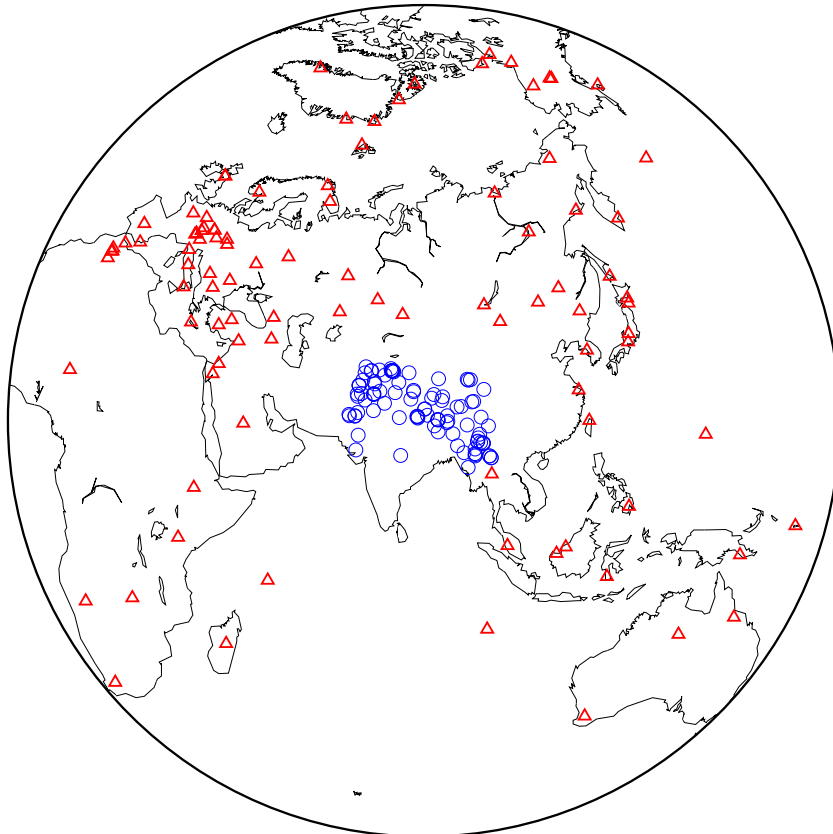

Fig. 4. Distribution of earthquakes (blue circles) and stations (red triangles) used in the study.

times, hence the average wave velocity in the source region. The typical values of crustal *Vp* and *Vs* range between 6.2 to 6.6 km/s and between 3.5 to 3.9 km/s. If the velocity reduces by 5% and the thickness of the crust increases by 5 km (Kennett et al., 1995; Mejia, 2001), the focal depth will move up by 2 km. There are some additional errors in arrival time readings and gCMT solutions. We infer that the uncertainties in focal depth determination are predominantly within ±3 km.

Fig. 5 shows two examples of seismic waveform modeling. Event S7 is a normal-faulting earthquake that occurred in the Lhasa terrane. The focal depth estimated from waveform modeling is 9 km. Corrections of 5 km for the topography give the focal depth of 4 km (Fig. 5(a)). Event S8 is a reverse-faulting earthquake with a strike-slip component. The final depth calculated is 40 km, which is 25 km deeper than the depth listed in the gCMT catalog (Fig. 5(b)).

3. Results

The focal depths and source parameters of 97 earthquakes investigated are given in Table 1 and Fig. 6. The focal depths of these earthquakes range from 2 to 49 km. All the earthquakes with focal depths greater than 20 km are located at the margin of the plateau. There is shortening in the north, shearing in the center, and underthrusting in the south, representing the Asian, Indian, and Tibetan lithospheric mantle, respectively. Therefore, we divide the study area into several different sub-
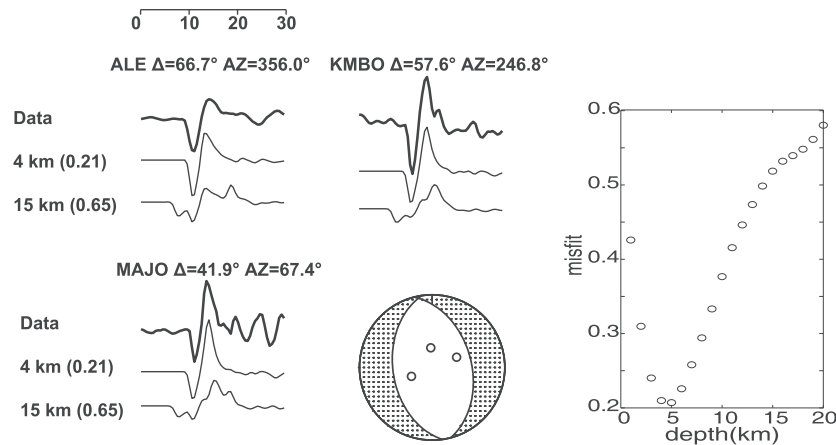
regions: northern Tibet, central Tibet, southern Tibet, and eastern and western Himalayan syntaxes.

3.1. Northern Tibet

Northern Tibet is defined as the region north of the Kunlun Suture and its western extension, including the Kunlun terrane, Tarim Basin, and Tien Shan mountain belt (Fig. 7). The Asian lithospheric mantle underplates southward beneath the northern Tibetan plateau with increasing angles from east to west (Willett and Beaumont, 1994; Kind et al., 2002; Schneider et al., 2013). The descending fronts marked by different studies vary. Nevertheless, it reaches far beneath the Kunlun Suture (blue region in Fig. 6; Zhao et al., 2010; Zhang et al., 2011). Fault plane solutions of most earthquakes indicate thrust faulting, distinguishing northern Tibet from central Tibet.

The Kunlun terrane is bounded by large-scale left-lateral strike-slip faults, the Altyn–Tagh fault to the northwest, Haiyuan fault to the northeast, and Kunlun fault to the south (Peltzer et al., 1989). However, thrust-faulting earthquakes are typical characteristic of Kunlun terrane. Tarim and Qaidam Basins occupy a major portion of the region so that the crust below northern Tibet is rather old and tough. The Moho depths beneath northern Tibet range from 50 to 60 km. Most earthquakes in this region are shallower than 30 km and thus located in the upper or middle crust.
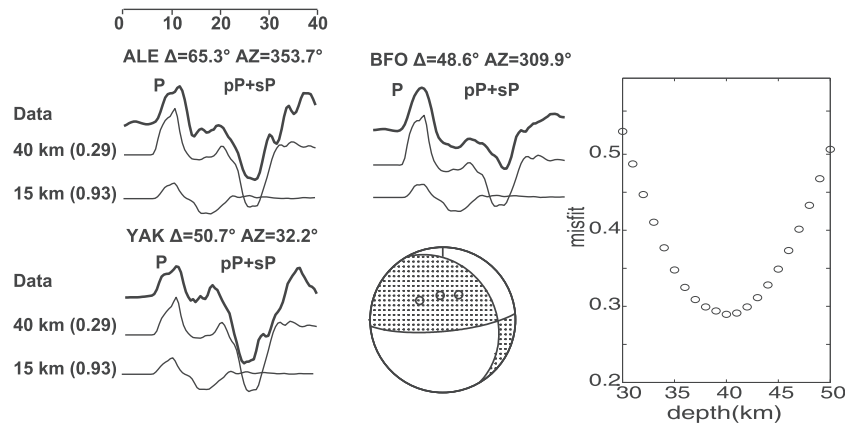

Fig. 5. Two examples of waveform modeling. The waveforms are (from top to bottom) the raw data, the synthetics at the preferred depth, and the synthetics at the depth listed in the gCMT catalog. The numbers in parentheses following the depth are least-squares misfit between observed and synthetic seismograms (see Bai et al., 2014 for the identification of the depth phases).

Table 1

Source parameters of 97 earthquakes obtained from teleseismic waveform modeling.

ID	Date yyyy-mm-dd	Time (GMT) hh:mm	λ_E /°	ψ_N /°	H /km	M_W	Fault plane Strike/Dip/Rake	Misfit	Moho /km
Northern Tibet									
N1	1993-10-02	08:42	88.66	38.17	11	6.1	326/42/146	0.28	50
N2	1997-04-05	23:46	76.88	39.54	18	5.9	161/78/(−172)	0.49	55
N3	1997-04-06	04:36	77.00	39.54	15	5.9	253/43/−36	0.31	55
N4	1997-04-11	05:34	76.95	39.56	17	6.1	240/37/(−82)	0.31	55
N5	1997-04-15	18:19	76.98	39.62	18	5.8	170/66/−162	0.42	55
N6	1998-03-19	13:51	76.73	39.92	26	5.6	243/23/(67)	0.64	55
N7	1998-05-28	21:11	78.87	37.39	14	5.6	95/9/63	0.52	53
N8	1998-08-02	04:40	77.03	39.57	16	5.6	231/30/(−91)	0.29	55
N9	1998-08-27	09:03	77.34	39.58	32	6.3	240/78/−44)	0.53	55
N10	2000-09-12	00:27	99.37	35.37	6	6.1	343/80/−170	0.56	60
N11	2003-02-24	02:03	77.23	39.61	30	5.7	239/33/69	0.50	55
N12	2003-03-12	04:47	77.43	39.36	12	5.4	245/33/79	0.42	55
N13	2003-04-17	00:48	96.48	37.53	9	6.2	294/29/91	0.35	60
N14	2003-09-01	23:16	75.32	38.60	4	5.7	107/47/−153	0.60	60
N15	2008-11-10	01:22	95.83	37.56	17	6.0	252/28/63	0.58	60
N16	2009-08-28	01:52	95.68	37.72	11	6.1	295/31/95	0.27	60
N17	2012-03-08	22:50	81.31	39.38	45	5.9	132/46/128	0.45	53
Central Tibet									
C1	1994-06-29	18:22	93.69	32.56	4	5.9	9/40/−105	0.20	75
C2	1996-11-19	10:44	78.20	35.31	14	6.8	180/71/170	0.51	65
C3	1997-11-08	10:02	87.37	35.12	10	7.5	348/88/(−168)	0.58	65
C4	2001-03-05	05:50	86.90	34.37	13	5.6	170/64/−153	0.52	65
C5	2003-07-07	06:55	89.47	34.61	15	5.7	60/81/6	0.53	70
C6	2004-03-27	18:47	89.18	33.95	7	5.9	187/44/−78	0.47	75
C7	2007-05-05	08:51	81.97	34.25	4	6.1	220/88/−36	0.64	65
C8	2008-01-09	08:26	85.17	32.29	8	6.3	206/46/−78	0.19	75
C9	2008-01-16	11:54	85.16	32.33	6	5.8	23/44/−102	0.46	75
C10	2010-03-24	02:06	92.70	32.50	8	5.6	162/74/−108	0.47	75
C11	2010-04-13	23:49	96.63	33.27	10	6.7	210/67/−164	0.35	70
C12	2010-05-29	02:30	96.25	33.25	20	5.6	75/88/11	0.69	70
C13	2012-08-12	10:47	82.52	35.67	12	6.2	215/47/−52	0.32	65
C14	2013-08-11	21:23	97.96	30.05	2	5.8	90/54/−40	0.42	65
C15	2013-08-31	00:04	99.35	28.24	4	5.7	97/42/−95	0.40	55
C16	2014-02-12	09:19	82.59	35.91	6	6.9	332/85/(−161)	0.55	65
Southern Tibet									
S1	1991-11-08	15:13	70.66	26.38	26	5.4	56/43/46	0.69	35
S2	1992-05-20	12:20	71.33	33.36	12	6.0	237/5/79	0.25	46
S3	1992-07-30	08:24	90.18	29.57	7	6.1	10/42/−94	0.32	70
S4	1993-01-18	12:42	90.38	30.84	5	5.9	25/48/−57	0.25	75
S5	1993-03-20	14:51	87.33	29.03	16	6.2	161/46/−121	0.50	70
S6	1996-04-01	08:08	73.46	31.46	40	5.2	98/33/101	0.76	50
S7	1996-07-03	06:44	88.19	30.11	4	5.6	172/45/−102	0.21	75
S8	1997-02-27	21:08	68.20	29.96	40	7.1	85/77/82	0.29	41
S9	1997-03-20	08:50	68.02	30.13	21	5.9	76/7/−91	0.47	41
S10	1997-05-08	02:53	92.28	24.89	36	5.9	347/86/(−167)	0.54	41
S11	1997-05-21	22:51	80.04	23.08	38	5.8	283/26/129	0.36	43
S12	1998-07-20	01:06	88.25	30.18	17	5.7	16/32/−83	0.54	75
S13	1998-08-25	07:41	88.16	30.27	20	5.8	14/46/−67	0.62	75
S14	1999-02-11	14:08	69.24	34.31	18	6.0	194/66/(−30)	0.66	38
S15	1999-03-28	19:05	79.42	30.51	16	6.5	280/7/75	0.57	70
S16	1999-06-26	21:54	69.45	30.05	15	5.5	18/47/41	0.62	60
S17	1999-07-12	03:42	69.46	29.99	19	5.6	269/60/152	0.53	41
S18	2001-01-28	01:02	70.52	23.51	14	5.7	286/43/100	0.24	35
S19	2002-07-13	20:06	69.98	30.80	30	5.5	171/66/18	0.42	41
S20	2004-07-11	23:08	83.67	30.69	4	6.3	359/45/−96	0.48	75
S21	2005-04-07	20:04	83.66	30.49	6	6.3	170/43/−67	0.25	75
S22	2005-06-01	20:06	94.63	28.88	19	5.6	209/6/28	0.34	65
S23	2005-10-08	10:46	73.10	34.73	8	6.1	328/39/77	0.46	60
S24	2005-10-08	12:25	73.12	34.77	3	5.9	96/47/39	0.85	60
S25	2005-10-09	08:30	73.18	34.67	6	5.7	344/37/122	0.27	60
S26	2008-08-25	13:21	83.52	30.90	14	6.3	30/48/−93	0.59	75
S27	2008-09-25	01:47	83.47	30.83	14	5.6	208/75/12	0.81	75
S28	2008-10-05	22:56	69.47	33.89	31	5.8	218/80/10	0.40	41
S29	2008-10-06	08:30	90.35	29.81	4	6.3	44/48/−75	0.30	70
S30	2009-07-24	03:11	85.86	31.12	20	5.4	318/74/170	0.67	75
S31	2009-09-21	08:53	91.42	27.35	13	6.0	281/6/99	0.52	65
S32	2011-09-18	12:40	88.15	27.80	49	6.9	216/72/(−8)	0.34	60
S33	2013-04-24	09:25	70.22	34.53	37	5.5	200/46/153	0.75	43
S34	2013-05-01	06:57	75.84	33.10	16	5.6	328/23/113	0.34	60

Table 1 (*continued*)

ID	Date yyyy-mm-dd	Time (GMT) hh:mm	λ_E /°	ψ_N /°	H /km	M_W	Fault plane Strike/Dip/Rake	Misfit	Moho /km
Western syntaxis									
W1	1992-05-10	04:04	72.93	37.17	5	5.8	186/45/−55	0.68	60
W2	1998-05-30	06:22	70.12	37.15	19	6.5	291/83/(179)	0.75	50
W3	2002-03-25	14:56	69.32	36.06	5	5.9	16/39/98	0.38	41
W4	2002-04-12	04:00	69.42	35.96	5	5.7	204/46/96	0.46	38
W5	2002-11-20	21:32	74.51	35.41	6	6.0	204/30/−91	0.54	65
W6	2004-11-17	20:58	71.86	39.19	6	5.8	185/88/11	0.65	50
W7	2006-07-06	03:57	71.82	39.13	5	5.8	285/59/145	0.52	50
W8	2007-01-08	17:21	70.31	39.80	9	6.1	187/65/16	0.40	50
W9	2008-10-05	15:52	73.82	39.53	4	6.4	246/38/102	0.35	60
W10	2012-03-12	06:06	73.15	36.74	6	5.7	212/53/(−5)	0.63	60
W11	2012-05-12	23:28	70.35	38.61	12	5.7	62/34/139	0.49	50
W12	2012-06-11	05:29	69.35	36.02	16	5.7	329/71/17	0.69	41
Eastern syntaxis									
E1	1992-04-23	14:18	98.93	22.43	9	6.1	354/77/−168	0.39	39
E2	1992-04-23	15:32	98.88	22.43	5	6.1	345/68/−173	0.61	39
E3	1992-06-15	02:48	95.97	24.00	15	6.3	8/69/−173	0.25	45
E4	1994-01-11	00:51	97.21	25.21	10	6.1	106/25/−85	0.60	43
E5	1994-04-06	07:03	96.84	26.16	11	5.8	96/57/26	0.55	55
E6	1994-05-29	14:11	94.18	20.54	12	6.5	316/86/−122	0.77	44
E7	1994-11-21	08:16	96.67	25.54	10	5.9	34/76/179	0.55	43
E8	1995-07-09	20:31	99.17	21.99	5	5.9	64/66/(−20)	0.58	45
E9	1995-07-11	21:46	99.20	21.98	20	6.8	330/89/(−164)	0.42	45
E10	1997-12-30	13:43	96.59	25.40	17	5.7	122/84/(−4)	0.68	43
E11	2000-06-07	21:46	97.19	26.80	13	6.3	290/38/41	0.52	55
E12	2008-08-21	12:24	97.68	25.04	9	5.9	7/80/173	0.40	43
E13	2012-11-11	10:54	95.83	22.72	5	5.9	91/75/14	0.49	43
E14	2012-11-11	18:19	95.87	23.13	28	5.6	358/71/167	0.61	43
E15	2013-09-20	12:24	95.96	22.93	10	5.7	95/74/(−2)	0.46	43
E16	2014-05-23	20:49	97.84	24.97	17	5.7	334/85/(−165)	0.70	43
E17	2014-05-30	01:20	97.85	25.00	7	5.9	82/79/(−8)	0.42	43
E18	2014-11-20	18:14	93.52	23.52	50	5.7	157/56/−150	0.58	41

ID is the number of earthquake in origin time order in each region. The date and origin time are GMT time. The epicenter (λ_E, and ψ_N), moment magnitude (M_W), strike and dip of the fault plane are taken from the gCMT catalog. The rake of the fault plane is either from the gCMT or from this study (shown in the parentheses) if the station coverage is good and the gCMT value is more than 10° different from this study. Misfit is least-square variance between observed and synthetic seismograms.

The event N17 in the Tarim basin presents an exception in that it originated in the lower crust. The relocated focal depth for this event is 46 km, which is only ca. 7 km above the Moho. As old basins are stable and earthquakes are rare (Sloan et al., 2011), we can hypothesize generation or reactivation of the fault because of the ongoing collision.
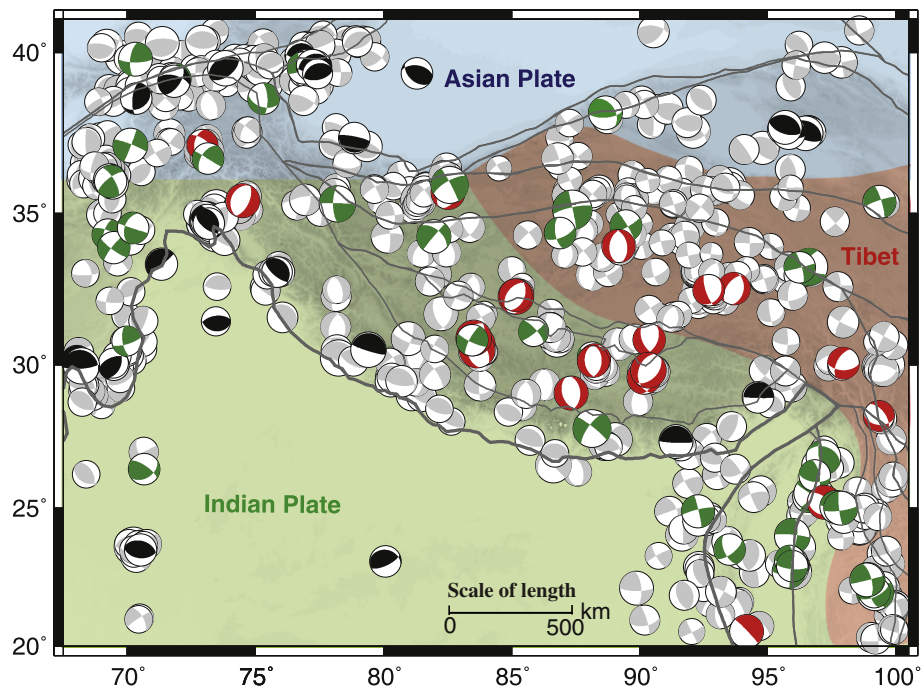

Fig. 6. Focal depths and focal mechanisms of shallow earthquakes obtained from waveform modeling. The black, red, and green beach balls are thrust, normal, and strike-slip faulting earthquakes, respectively. Gray beach balls are those taken from the gCMT catalog. The background marked by the blue, pink, and green show locations of the Asian, Tibetan, and Indian lithospheres, respectively.
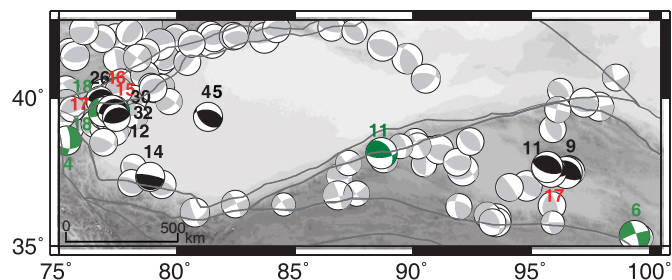
Fig. 7. Focal depths and mechanisms for earthquakes in northern Tibet. The black, red, and green beach balls are thrust, normal, and strike-slip faulting earthquakes, respectively. The numbers beside them are the corresponding focal depths.

3.2. Central Tibet

Central Tibet is defined as the region between the Bangong-Nujiang and Kunlun Sutures, including Songpan-Ganzi and Qiangtang terranes (Fig. 8). This region is primarily composed of Tibetan lithosphere, which behaves like a deformable crush zone between the colliding plates (pink region in Fig. 6; Zhao et al., 2010). The dominant mode of crustal deformation in this region is pure shear thickening.

Crustal flow has been proposed as a mechanism for the southeast-ward extrusion of the plateau (Solid arrows in Fig. 8; Royden et al., 1997; Beaumont et al., 2004; Klemperer, 2006). This model was origi-nally established on the basis of numerical simulation and later con-firmed by the geophysical observations of low-velocity and high-conductivity layers (Yuan et al., 1997; Bai et al., 2010; Yang et al., 2012). The lithosphere is warm and weak marked as strong attenuation of Sn wave traveling in the uppermost mantle and large seismic anisot-ropy (dotted line in Fig. 8; McNamara et al., 1997; Soto et al., 2012; Searle, 2013; Zhang et al., 2015). Cenozoic high potassic volcanic rocks and lower crustal xenoliths are rich in the middle and lower crust at depths of 30–50 km (Hacker et al., 2000; Tilmann et al., 2003), suggest-ing partial melting in the lower crust caused by the elevated tempera-ture as a result of the plate convergence.

In agreement with previous observations, we found no earthquakes located in the lower crust. The relocated focal depths for 17 earthquakes range between 2 and 20 km. They are most likely concentrated within the upper layer of the crust because the Moho in this region ranges be-tween 65 and 80 km. The lower crust beneath central Tibet does not seem cold enough to allow the seismogenic zone to extend to such depths.
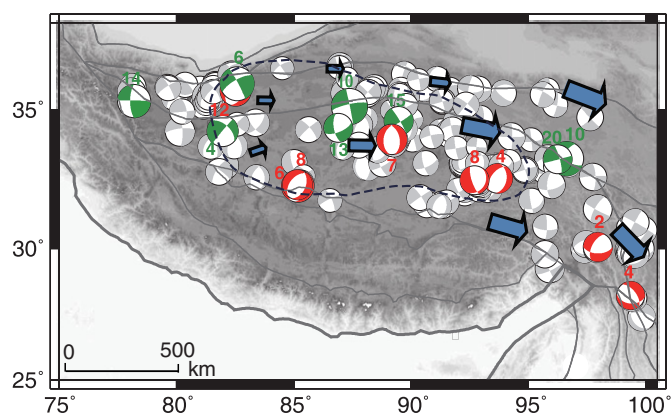

Fig. 8. Focal depths and mechanisms for earthquakes in central Tibet. The solid arrows rep-resent the direction and the strength of lower crustal flow (Klemperer, 2006; Cao et al., 2013). The black dashed line indicates the strong Sn wave attenuation zone (McNamara et al., 1997).

3.3. Southern Tibet

This region represents the area south of Bangong-Nujiang Suture, in-cluding the Lhasa terrane, Himalayas, and northern part of the Indian shield (Fig. 9). Its tectonics is primarily controlled by the descending pro-cess of the Indian plate beneath southern Tibet (green area in Fig. 6). The northward subduction of the Indian plate reaches up to 200 km beneath Tibet, with a front located beneath the Bangong-Nujiang Suture (Kosarev et al., 1999; Xu et al., 2015).

Although earthquakes certainly occur in the oceanic mantle, earth-quakes in the continental lithospheric mantle are known to be rare (Chen and Yang, 2004; Priestley et al., 2008). Several earthquakes we studied are deeper than 35 km (No. S6, S8, S11, and S32). The deepest one is a strike-slip earthquake, which is located in the northwest of Himalayan main boundary thrust (No. S32). Its focal depth is 49 km, which is ca. 10 km shallower than the average value of the mantle depth estimated by wide-angle reflection and refraction studies (Jackson et al., 2008). All these earthquakes are likely to be located in the lower crust of the subducted Indian plate because there might be hydrous materials at temperatures less than 600 °C (Jackson et al., 2008; Priestley et al., 2008; Craig et al., 2012).

Whether the crustal flow exists beneath the E–W trending central Himalaya or not is still controversial (Beaumont et al., 2004; Copley et al., 2011). The topography in southern Tibet and Himalayas is great, leading to different crustal structures from those in central Tibet. Most earthquakes in this region are shallower than 20 km and one earthquake is located at 49 km (No. S32). We infer that if the crustal flow exists, it takes place at the greater depths within the overriding Tibetan crust.

3.4. Pamir-Hindu Kush and Indo-Burma deep subduction zones

The Pamir-Hindu Kush is also called western Himalayan syntaxis, which consists of Pamir to the north, Hindu-Kush to the west, and Karakoram Fault to the east (upper left corner in Fig. 6). This region is characterized by extreme shortening of the upper crust and strong in-teraction of various layers of lithosphere. It is by far the most active re-gion of intermediate-depth seismicity in the world not obviously associated with oceanic subduction (Pegler and Das, 1998; Bai and Zhang, 2015). The crustal shortening caused by the northward com-pression of the Pamir occurs mainly along the Main Pamir Thrust, par-tially consuming a portion of energy of Indian and Asian plate convergence (Reigber et al., 2001; Mohadjer et al., 2010; Zubovich et al., 2010; Ischuk, 2011; Ischuk et al., 2013; Sui et al., 2015). Many shallow earthquakes occurred at the Main Pamir Thrust at focal depths of 4–19 km, while intermediate-deep earthquakes are mostly located at the Hindu-Kush below 75 km.

The Indo-Burma region is located south of the eastern Himalayan syntaxis, where the strike of the plate boundary suddenly changes from nearly E-W at the Himalayas to nearly NS at the Burma Arc (lower right corner in Fig. 6; Reddy et al., 2009; Zhang et al., 2012). The largest earth-quake of the region ever recorded by China in the recording history is the Assam–Tibet earthquake of Mw = 8.6 on August 15, 1950 (Khattri and Wyss, 1987). The Burma arc subduction zone is a typical oblique plate convergence zone (Chen and Molnar, 1990; Satyabala, 2003), the eastern boundary is the north–south striking dextral Sagaing fault, which hosts many of the shallow earthquakes. The focal depths are less than 22 km. In contrast, focal mechanisms of the intermediate-depth earthquakes along the subduction zone reflect east–west trending reverse faulting (Chen and Molnar, 1990; Satyabala, 2003).

4. Discussion and conclusions

The Tibetan plateau is one of the most active regions of continental earthquakes in the world. Shallow seismicity is widespread over the plateau, while intermediate-depth earthquakes are dominant in the eastern and western Himalayan syntaxes. Published catalog locations
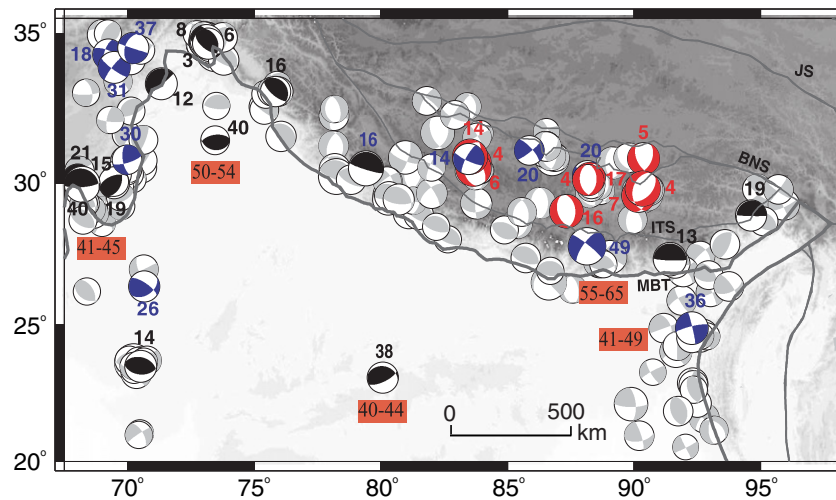
Fig. 9. Focal depths and mechanisms for earthquakes in southern Tibet. Numbers with red background show Moho depth imaged by seismic refraction or wide-angle reflection data.

indicate a random distribution of shallow events, inconsistent with the proposed tectonic models for the evolution history of the Tibetan plateau. A detailed investigation of moderate-sized earthquakes using waveform modeling indicates that only a few events are actually deeper than 20 km and all of them are located near the edges of the plateau.

All the 97 earthquakes studied are located within the crust. However, the variation patterns of focal depths and mechanisms are not exactly consistent with the horizontal inhomogeneity marked by different terranes. Some of the sutures which separate each terrane are no longer active and have been reconstructed by the plate collision and subduction. The Asian plate passively subducts beneath northern Tibet, where thrust-faulting earthquakes are dominant. These earthquakes occurred at the lower crust of the Tarim Basin and at the upper and middle crust at the margins of the Tarim Basin. In central Tibet, which is primarily underlain by the Tibetan lithosphere, earthquakes are typically strike-slip and mostly located within the upper crust, in agreement with the low-velocity layers and strong Sn attenuation zones observed previously at the lower crust. Earthquakes occurred beneath the Himalaya tend to be as deep as 40–50 km, consistent with the idea of

geothermal gradient reversal caused by deep subduction of the Indian plate (Shi and Zhu, 1993).

Nearly 40% of earthquakes with waveforms available on the IRIS DMC are intermediate-depth earthquakes, which are all located at the eastern and western Himalayan syntaxes. The issue of intermediate-depth earthquakes has been discussed in a separate study (Bai and Zhang, 2015). In brief, the intermediate-depth earthquakes in the Pamir-Hindu Kush and Indo-Burma regions reflect the ongoing deformation along the plate interface. The continental slab beneath the Indian-Eurasian collision zone deforms in a more complex manner than the oceanic slab subduction, combining tension, shearing, and oblique convergence with plate subduction.

To better constrain the seismogenic thickness (*Ts*) of the study region, we have incorporated focal depths of an additional 127 moderate earthquakes into this study. These 127 earthquakes have either occurred before 1990 (Molnar and Chen, 1983; Baranowski et al., 1984; Molnar and Lyon-Caen, 1989; Chung, 1993; Fan et al., 1994; Chen and Yang, 2004; Monsalve et al., 2006; Sloan et al., 2011), in the surroundings of the study region (Nelson et al., 1987; Sloan et al., 2011), or
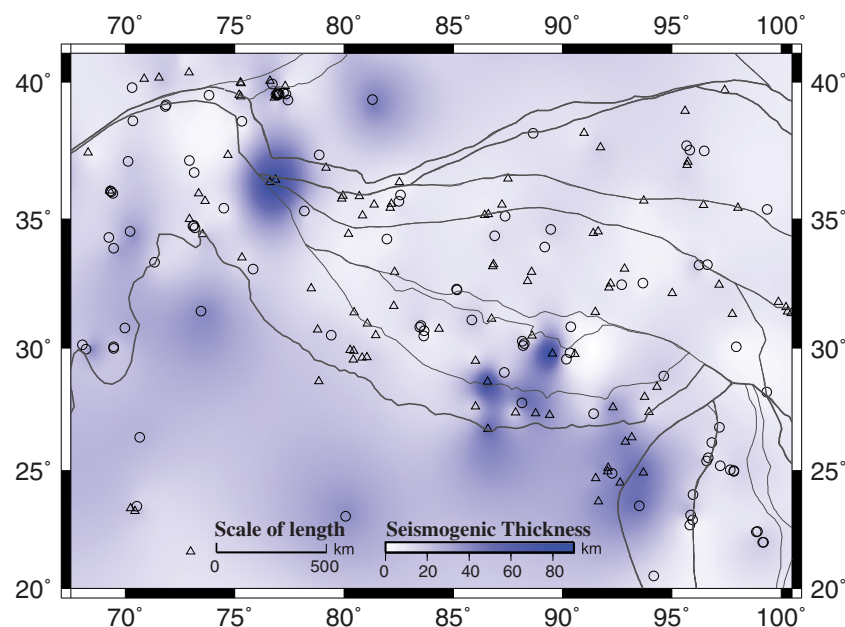

Fig. 10. Seismogenic thickness estimated based on relocated focal depths of 224 moderate earthquakes from this study (black circles) and from previous studies (black triangles).

after 1990 with waveforms unavailable on the IRIS website (Cotton et al., 1996; Ghose et al., 1998; Mitra et al., 2005; Sloan et al., 2011; Craig et al., 2012). The pattern of Ts (Fig. 10) is plotted using GMT surface (Wessel and Smith, 1995), based on a modified standard minimum curvature algorithm. A 0.1° radius has been used for sampling and gridding in order to eliminate large variations. The Ts is particularly high for southern Tibet and the southeastern Tarim Basin compared to that of the typical values for central and northeastern Tibet. For central Tibet, the observed Ts is consistent with the effective elastic thickness (Te) (Jordan and watts, 2005) and both the Ts and Te are less than 20 km. The Ts and Te are not comparable for southern Tibet because of multiple elastic layers beneath the area. The Ts is found to be highly variable along the strike of the Himalayan foreland, especially around central and eastern portion, where the 2015 M_W7.8 Gorkha, Nepal, earthquake occurred.

Acknowledgements

References

Amante, C., Eakins, B.W., 2009. ETOPO1 1 Arc-Minute Global Relief Model: Procedures, Data Sources and Analysis. NOAA Technical Memorandum NESDIS NGDC-24. National Geophysical Data Center, NOAA http://dx.doi.org/10.7289/V5C8276M.

Bai, L., Zhang, T., 2015. Complex deformation pattern of the Pamir–Hindu Kush region inferred from multi-scale double-difference earthquake relocations. Tectonophysics 638, 177–184.

Bai, D., Unsworth, M.J., Meju, M.A., Ma, X., Teng, J., Kong, X., Sun, Y., Sun, J., Wang, L., Jiang, C., Zhao, C., Xiao, P., Liu, M., 2010. Crustal deformation of the eastern Tibetan plateau revealed by magnetotelluric imaging. Nature Geoscience 3, 358–362.

Bai, L., Medina Luna, L., Hetland, E., Ritsema, J., 2014. Focal depths and mechanisms of Tohoku-Oki aftershocks from teleseismic P wave modeling. Earthquake Science 27, 1–13. http://dx.doi.org/10.1007/s11589-013-0036-x.

Baranowski, J., Armbruster, J., Seeber, L., Molnar, P., 1984. Focal depths and fault plane solutions of earthquakes and active tectonics of the Himalaya. Journal of Geophysical Research 89 (B8). http://dx.doi.org/10.1029/JB089iB08p06918.

Bassin, C., Laske, G., Masters, G., 2000. The current limits of resolution for surface wave tomography in North America. Eos, Transactions American Geophysical Union 81, F897.

Beaumont, C., Jamieson, R.A., Nguyen, M.H., Medvedev, S., 2004. Crustal channel flows: 1. Numerical models with applications to the tectonics of the Himalayan–Tibetan orogen. Journal of Geophysical Research 109, B06406. http://dx.doi.org/10.1029/2003JB002809.

Cao, J., Wang, H., Shi, Y., 2013. Numerical modeling of lower crustal flow beneath the Tibetan Plateau. Earthquake 33, 55–63 (in Chinese with English abstract).

Chen, W.P., Molnar, P., 1990. Source parameters of earthquakes and intraplate deformation beneath the Shillong Plateau and the northern Indoburman ranges. Journal of Geophysical Research 95 (B8), 12527–12552.

Chen, W.P., Yang, Z.H., 2004. Earthquakes beneath the Himalayas and Tibet: evidence for strong lithospheric mantle. Science 304 (5679), 1949–1952. http://dx.doi.org/10.1126/science.1097324.

Chung, W., 1993. Source parameters of two rift-associated intraplate earthquakes in peninsular India: the Bhadrachalam earthquake of April 13, 1969 and the Broach earthquake of March 23, 1970. Tectonophysics 225 (3), 219–230.

Copley, A., Avouac, J.P., Wernicke, B.P., 2011. Evidence for mechanical coupling and strong Indian lower crust beneath southern Tibet. Nature 472 (7341), 79–81.

Cotton, F., Campillo, M., Deschamps, A., Rastogi, B., 1996. Rupture history and seismotectonics of the 1991 Uttarkashi, Himalaya earthquake. Tectonophysics 258 (1-4), 35–51.

Craig, T.J., Copley, A., Jackson, J., 2012. Thermal and tectonic consequences of India underthrusting Tibet. Earth and Planetary Science Letters 353–354, 231–239.

Ekström, G., Nettles, M., Dziewoński, A.M., 2012. The global CMT project 2004–2010: Centroid-moment tensors for 13,017 earthquakes. Physics of the Earth and Planetary Interiors 200, 1–9.

Engdahl, E.R., Hilst, R., Buland, R., 1998. Global teleseismic earthquake relocation with improved travel times and procedures for depth determination. Bulletin of the Seismological Society of America 88, 722–743.

Fan, G., Ni, J., Wallace, T., 1994. Active tectonics of the Pamirs and Karakorum. Journal of Geophysical Research 99 (B4), 7131–7160.

Ghose, S., Hamburger, M., Virieux, J., 1998. Three-dimensional velocity structure and earthquake locations beneath the Northern Tien Shan of Kyrghzstan, central Asia. Journal of Geophysical Research 103, 2725–2748.

Hacker, B.R., Gnos, E., Ratschbacher, L., Grove, M., McWilliams, M., Sobolev, S.V., Jiang, W., Wu, Z., 2000. Hot and dry xenoliths from the lower crust of Tibet. Science 287, 2463–2466.

Hatzfeld, D., Molnar, P., 2010. Comparisons of the kinematics and deep structures of the zagros and himalaya and of the iranian and Tibetan plateaus and geodynamic implications. Reviews of Geophysics 48, RG2005. http://dx.doi.org/10.1029/2009RG000304.

Ischuk, A., 2011. Usoi rockslide dam and Lake Sarez, Pamir Mountains, Tajikistan. Natural and artificial rockslide dams. Lecture Notes in Earth Sciences 133, 423–440.

Ischuk, A., Bendick, R., Rybin, A., Molnar, P., Khan, S.F., Kuzikov, S., Mohadjer, S., Saydullaev, U., Ilyasova, Z., Schelochkov, G., Zubovich, A.V., 2013. Kinematics of the Pamir and Hindu Kush regions from GPS geodesy. Journal of Geophysical Research 118, 2408–2416. http://dx.doi.org/10.1002/jgrb.50185.

Jackson, J., McKenzie, D., Priestley, K., Emmerson, B., 2008. New views on the structure and rheology of the lithosphere. Journal of the Geological Society, London 165, 453–465.

Jordan, T.A., Watts, A.B., 2005. Gravity anomalies, flexure and the elastic thickness structure of the India-Eurasia collisional system. Earth and Planetary Science Letters 236, 732–750.

Kennett, B.L.N., Engdahl, E.R., Buland, R., 1995. Constraints on seismic velocities in the Earth from traveltimes. Geophysical Journal International 122 (1), 108–124.

Khattri, K., Wyss, M., 1987. Precusory variation of seismicity rate in Assam area, India. Geology 6, 685–688.

Kikuchi, M., Kanamori, H., 1982. Inversion of complex body waves-II. Physics of the Earth and Planetary Interiors 43, 205–222.

Kind, R., Yuan, X., Saul, J., Nelson, D., Sobolev, S., Mechie, J., Zhao, W., Kosarev, G., Ni, J., Achauer, U., Jiang, M., 2002. Seismic images of crust and upper mantle beneath Tibet: evidence for Eurasian plate subduction. Science 298 (5596), 1219–1221.

Klemperer, S.L., 2006. Crustal flow in Tibet: geophysical evidence for the physicalstate of Tibetan lithosphere, and inferred patterns of active flow. Geological Society, London, Special Publications 268, 39–70.

Kosarev, G., Kind, R., Sobolev, S.V., Yuan, X., Hanka, W., Oreshin, S., 1999. Seismic evidence for a detached Indian lithospheric mantle beneath Tibet. Science 283 (5406), 1306–1309.

Maggi, A., Jackson, J.A., Priestley, K., Baker, C., 2000. A reassessment of focal depth distributions in southern Iran, the Tien Shan and northern India: do earthquakes really occur in the continental mantle? Geophysical Journal International 143, 629–661.

McNamara, D.E., Walter, W.R., Owens, T.J., Ammon, C.J., 1997. Upper mantle velocity structure beneath the Tibetan Plateau from Pn travel time tomography. Journal of Geophysical Research 102, 493–505. http://dx.doi.org/10.1029/96JB02112.

Mejia, J.A., 2001. Lithospheric structure beneath the Tibetan plateau using simultaneous inversion of surface wave dispersion and receiver functions. Saint Louis University (333 pp.).

Mitra, S., Priestley, K., Bhattacharyya, A., Gaur, V.K., 2005. Crustal structure and earthquake focal depths beneath northeastern India and southern Tibet. Geophysical Journal International 160, 227–248.

Mohadjer, S., Bendick, R., Ischuk, A., Kuzikov, S., Kostuk, A., Saydullaev, U., Lodi, S., Kakar, D.M., Wasy, A., Khan, M.A., Molnar, P., Bilham, R., Zubovich, A.V., 2010. Partitioning of India-Eurasia convergence in the Pamir-Hindu Kush from GPS measurements. Geophysical Research Letters 37, L04305. http://dx.doi.org/10.1029/2009GL041737.

Molnar, P., Chen, W., 1983. Focal depths and fault plane solutions of earthquakes under the Tibetan plateau. Journal of Geophysical Research 88 (B2), 1180–1196.

Molnar, P., Lyon-Caen, H., 1989. Fault plane solutions of earthquakes and active tectonics of the Tibetan Plateau and its margins. Geophysical Journal International 99 (1), 123–154.

Monsalve, G., Sheehan, A., Schulte-Pelkum, V., Rajaure, S., Pandey, M., Wu, F., 2006. Seismicity and one-dimensional velocity strcture of the Himalayan collision zone: earthquakes in the crust and upper mantle. Geophysical Research 111. http://dx.doi.org/10.1029/2005JB004062.

Nelson, M., McCaffrey, R., Molnar, P., 1987. Source parameters for 11 earthquakes in the Tien Shan, central Asia, determined by P and SH waveform inversion. Journal of Geophysical Research 92 (B12). http://dx.doi.org/10.1029/JB092iB12p12629.

Pegler, G., Das, S., 1998. An enhanced image of the Pamir Hindu Kush seismic zone from relocated earthquake hypocentres. Geophysical Journal International 134 (2), 573–595. http://dx.doi.org/10.1046/j.1365-246x.1998.00582.x.

Peltzer, G., Tapponnier, P., Armijo, R., 1989. Magnitude of Late Quaternary left-lateral displacements along the north edge of Tibet. Science 246 (4935), 1285–1289.

Priestley, K., Jackson, J., McKenzie, D., 2008. Lithospheric structure and deep earthquakes beneath India, the Himalaya and southern Tibet. Geophysical Journal International 172 (1), 345–362. http://dx.doi.org/10.1111/j.1365-246X.2007.03636.x.

Rai, S.S., Priestley, K., Gaur, V.K., Mitra, S., Singh, M.P., Searle, M., 2006. Configuration of the Indian Moho beneath the NW Himalaya and Ladakh. Geophysical Research Letters 33, L15308. http://dx.doi.org/10.1029/2006GL026076.

Reddy, D.V., Nagabhushanam, P., Kumar, D., Sukhija, B.S., Thomas, P.J., Pandey, A.K., Sahoo, R.N., Prasad, G.V.R., Datta, K., 2009. The great 1950 Assam Earthquake revisited: field evidences of liquefaction and search for paleoseismic events. Tectonophysics 474 (3–4), 463–472. http://dx.doi.org/10.1016/j.tecto.2009.04.024.

Reigber, C., Michel, G.W., Galas, R., Angermann, D., Klotz, J., Chen, J.Y., Papschev, A., Arslanov, R., Tzurkov, V.E., Ishanov, M.C., 2001. New space geodetic constraints on the distribution of deformation in Central Asia. Earth and Planetary Science Letters 191, 157–165.

Royden, L.H., Burchfiel, B.C., King, R.W., Wang, E., Chen, Z., Shen, F., Liu, Y., 1997. Surface deformation and lower crustal flow in eastern Tibet. Science 276, 788–790. http://dx.doi.org/10.1126/science.276.5313.788.

Satyabala, S.P., 2003. Oblique plate convergence in the Indo-Burma (Myanmar) subduction region. Pure and Applied Geophysics 160 (9), 1611–1650. http://dx.doi.org/10.1007/s00024-003-2378-0.

Schneider, F.M., Yuan, X., Schurr, B., Mechie, J., Sippl, C., Haberland, C., Minaev, V., Oimahmadov, I., Gadoev, M., Radjabov, N., Abdybachaev, U., Orunbaev, S., Negmatullaev, S., 2013. Seismic imaging of subducting continental lower crust beneath the Pamir. Earth and Planetary Science Letters 375, 101–112.

Searle, M., 2013. Crustal melting, ductile flow, and deformation in mountain belts: cause and effect relationships. Lithosphere http://dx.doi.org/10.1130/RF.L006.1.

Shi, Y., Zhu, Y., 1993. Some thermotectonic aspects of the Tibetan Plateau. Tectonophysics 210, 223–233.

Shin, Y.H., Shum, C.K., Braitenberg, C., Lee, M.S., Xu, H., Choi, K.S., Baek, J.H., Jong, U.P., 2009. Three-dimensional fold structure of the Tibetan Moho from GRACE gravity data. Geophysical Research Letters 36, L01302. http://dx.doi.org/10.1029/2008GL036068.

Sloan, R.A., Jackson, J.A., McKenzie, D., Priestley, K., 2011. Earthquake depth distributions in central Asia, and their relations with lithosphere thickness, shortening and extension. Geophysical Journal International 185, 1–29.

Soto, G.L., Sandvol, E., Ni, J., Flesch, L., Hearn, T., Tilmann, F., Chen, J., Brown, L., 2012. Significant and vertically coherent seismic anisotropy beneath eastern Tibet. Journal of Geophysical Research 117. http://dx.doi.org/10.1029/2011JB008919.

Sui, Y., Zhou, Y., Wang, X., 2015. The effects of stagnant slabs on the topography of 410 km siscontinuity beneath the Pamir-Hindu Kush region. Chinese Journal of Geophysics 58, 149–157. http://dx.doi.org/10.1002/cjg2.20162.

Tilmann, F., Ni, J., Team, I.I.S., 2003. Seismic imaging of the downwelling Indian lithosphere beneath central Tibet. Science 300, 1424–1427. http://dx.doi.org/10.1126/science.1082777.

Wessel, P., Smith, W.H., 1995. New version of the generic mapping tools. Eos, Transactions American Geophysical Union 76 (33), 329.

Willett, S.D., Beaumont, C., 1994. Subduction of Asian lithospheric mantle beneath Tibet inferred from models of continental collision. Nature 369 (6482), 642–645.

Xu, Q., Zhao, J.M., Yuan, X.H., Liu, H.B., Pei, S.P., 2015. Mapping crustal structure beneath southern Tibet: seismic evidence for continental crustal underthrusting. Gondwana Research 27, 1487–1493.

Yang, Y., Ritzwoller, M.H., Zheng, Y., Shen, W., Levshin, A.L., Xie, Z., 2012. A synoptic view of the distribution and connectivity of the midcrustal low velocity zone beneath Tibet. Journal of Geophysical Research 117, B04303. http://dx.doi.org/10.1029/2011JB008810.

Yin, A., Harrison, T.M., 2000. Geologic evolution of the Himalayan–Tibetan orogen. Annual Review of Earth and Planetary Sciences 28, 211–280. http://dx.doi.org/10.1146/annurev.earth.28.1.211.

Yuan, X., Ni, J., Kind, R., Mechie, J., Sandvol, E., 1997. Lithospheric and upper mantle structure of southern tibet from a seismological passive source experiment. Journal of Geophysical Research 102 (B12), 27491–27500.

Zhang, Z., Klemperer, S., Bai, Z., Chen, Y., Teng, J., 2011. Crustal structure of the Paleozoic Kunlun orogeny from an active-source seismic profile between Moba and Guide in East Tibet, China. Gondwana Research 19, 994–1007.

Zhang, Z., Dong, X., Santosh, M., Liu, F., Wang, W., Yiu, F., He, Z., Shen, K., 2012. Petrology and geochronology of the Namche Barwa Complex in the eastern Himalayan syntaxis, Tibet: constraints on the origin and evolution of the north-eastern margin of the Indian Craton. Gondwana Research 21, 12–137.

Zhang, H., Zhao, D., Zhao, J., Liu, H., 2015. Tomographic imaging of the underthrusting Indian slab and mantle upwelling beneath central Tibet. Gondwana Research 28, 121–132.

Zhao, J., Yuan, X., Liu, H., Kumar, P., Pei, S., Kind, R., Zhang, Z., Teng, J.W., Ding, L., Gao, X., et al., 2010. The boundary between the Indian and Asian tectonic plates below Tibet. Proceedings of the National Academy of Sciences of the United States of America 107 (25), 11229–11233. http://dx.doi.org/10.1073/pnas.1001921107.

Zubovich, A.V., Wang, X., Scherba, Y.G., Schelochkov, G.G., Reilinger, R., Reigber, C., Mosienko, O.I., Molnar, P., Michajljow, W., Makarov, V.I., et al., 2010. GPS velocity field for the Tien Shan and surrounding regions. Tectonics 29, TC6014. http://dx.doi.org/10.1029/2010TC002772.